Supporting Information

Rodriguez et al. 10.1073/pnas.1213569110

SI Methods

Photophysical Properties of FFN102. UV absorption spectra of FFN102 were measured on a Molecular Devices SpectraMax Plus 384 UV/VIS spectrophotometer operated by SOFTmax software. Fluorescence measurements were acquired on a Jobin Yvon Fluorolog fluorescence spectrofluorometer. Absorption spectra were acquired for a final probe concentration of 20 μM in PBS with adjusted pH (2–10). Fluorescence measurements were taken of a final probe concentration of 20 μM in PBS with adjusted pH (7.4 or 5.0).

Imaging of FFN102. For striatal slices, images were captured in 16-bit 45.1 × 45.1-μm field of view (FOV) at 512 × 512-pixel resolution and a dwell time of 20–30 μs/pixel using the Prairie View software. For dopaminergic neurons, images were captured in 16-bit 112 × 112-μm FOV at 1,024 × 1,024 pixel resolution.

Imaging FFN102 with GFP. After probe incubation, striatal slices of TH-GFP animals (1) were imaged by two-photon microscopy using a Leica DM6000 with a titanium–sapphire MaiTai laser (Spectra-Physics) equipped with a 40×, 0.8 N.A. water-immersion objective. GFP fluorescence was detected using an excitation of 900 or 910 nm and an emission range of 510–580 nm, whereas FFN102 fluorescence was detected using an excitation of 760 nm and an emission range of 430–470 nm. Single *z*-plane images at each of the corresponding wavelengths were obtained using the LASAF software. To account for shifts in the *z* plane, a sequence of images was acquired in the following order: 1, FFN102; 2, GFP; and 3, FFN102. Colocalization between FFN102 in images 1 and 3, was used to determine the extent of *z* shifting and only sets of images with a colocalization of 92% or more, were used for the analysis of GFP and FFN102 colocalization.

To obtain accurate colocalization values, besides selecting image sequences with negligible shift in the *z* plane, it is important to maximize the signal of both fluorophores at an optimal range and confirm that the objective used provides an appropriate correction for chromatic aberration. Also, it is key to confirm that no crossover occurs between the two channels at the exact conditions used for image acquisition of FFN102-GFP image sequences. To do this, we confirmed a lack of signal in the FFN102 and GFP channels in TH-GFP slices not incubated with FFN102 and in wild-type slices incubated with FFN102, respectively.

6-Hydroxydopamine Injection. Under ketamine/xylazine/saline (1:1:4, 0.15–0.20 mL, i.p.) anesthesia, mice were placed in a stereotaxic frame (Kopf). Unilateral injection of the left hemisphere with 6-hydroxydopamine (6-OHDA) (3 mL of a 5 mg/mL 0.9% NaCl solution containing 0.02% ascorbic acid; animals received a total of 15 mg of 6-OHDA) was performed in the dorsal striatum (coordinates with respect to the bregma: anteroposterior, +0.9 mm; mediolateral, +2.2 mm; dorsoventral, −2.5 mm) using a Bee-stinger gastight syringe. 6-OHDA was injected using a Harvard Apparatus peristaltic pump at a rate of 0.5 mL/min. After injection, the needle was left in place for 5 min before slowly retracting to prevent reflux. The right hemisphere was left intact as a control.

Uptake Inhibition of FFN102 by Cocaine and Nomifensine. Mouse dorsal striatal slices were pretreated with DAT inhibitors [1 μM nomifensine or 5 μM cocaine in artificial cerebrospinal fluid (ACSF)] for a period of 10 min. After incubation with the corresponding inhibitor, slices were transferred to an ACSF solution containing 10 μM FFN102 and the corresponding inhibitor and incubated for 30 min before imaging. As a control, slices from the same animal but not treated with DAT inhibitors, were incubated for 30 min with 10 μM FFN102 and imaged using the same acquisition parameters as those used to image slices treated with the inhibitors.

Release of FFN102 by Amphetamine. After incubation with FFN102, dorsal striatal slices were placed in the recording chamber and perfused with ACSF. After acquiring an initial image ($t = 0$), perfusion was switched to ACSF containing 1 μM amphetamine (AMPH) and images acquired every 3 min for a total of 9 min. As a control, slices labeled with FFN102 were imaged over time in the absence of AMPH.

For midbrain slices, after incubation with FFN102, slices were moved to the recording chamber and continuously perfused with ACSF for 15 min. Images were acquired at 0, 20, and 40 min thereafter. One-half of the slices were perfused with ACSF containing 10 μM AMPH during the 20- to 40-min period, whereas the other half were perfused with regular ACSF throughout the entire experiment.

Destaining of FFN102 by KCl. Potassium depolarization-induced release was monitored by performing time-lapse image acquisition of FFN102-labeled slices before and during exposure to ACSF containing 40 mM KCl (solution prepared by isotonic replacement of NaCl). To account for shifts in the *z* plane, 3.0-μm *z* stacks composed of seven images, each image taken at 0.5-μm intervals, were taken over time. One *z* section representing the same field of view was then selected before and after exposure to high K^+ concentration. As a control, *z*-stack images of slices not perfused with high KCl were acquired over a similar time period. To confirm the calcium dependence of FFN102 release, slices were treated with 200 μM $CdCl_2$ for 20 min, followed by perfusion of ACSF containing 40 mM KCl and 200 μM $CdCl_2$.

Destaining of FFN102 by Electrical Stimulation. FFN102-labeled slices were placed on the imaging chamber and allowed to stabilize and wash for 15–20 min in oxygenated [95% O_2, 5% CO_2 (vol/vol)] ACSF containing the AMPA and NMDA receptor inhibitors NBQX (10 μM) and AP-5 (50 μM), respectively. Slices were then imaged for 140 s (15 time points, T1–T15) in the absence of exogenously applied stimuli. At this time, a 10-Hz stimulus (each pulse 600 μs × 150–200 μA) was applied locally to the dorsal striatum for 300 s during which image acquisition was continued for 30 more time points (T16–T45). Stimulation was locally applied by an Iso-Flex stimulus isolator triggered by a Master-8 pulse generator (AMPI), using stainless-steel bipolar electrodes. Control experiments were performed in the same manner as described above but in the absence of stimulation. For experiments with 200 μM $CdCl_2$, cadmium was present for 20 min before imaging and throughout the experiment. Images were captured in 16-bit 22.5 × 22.5-μm FOV at 256 × 256-pixel resolution and a dwell time of 12 μs/pixel using the Prairie View software. To compensate for shifts in the *z* plane, 2.5-μm *z* stacks composed of six images, each image taken at 0.5-μm intervals, were taken over time (before and during stimulation), and *z* sections representing the same field of view were selected for all time points for quantification. Each *z* stack was captured over a period of 10 s and the whole time course was acquired in ∼9 min.

Electrochemical Recordings in Striatal Slices. Striatal dopamine release was studied using fast-scan cyclic voltammetry. Recordings

were obtained from the first three coronal slices (300 μm), prepared from rostral caudate putamen. Slices were allowed to recover for 1.5 h in a holding chamber with ACSF at room temperature, and then placed in a recording chamber, and superfused (1 mL/min) with ACSF at 36 °C. Electrochemical recordings and electrical stimulation were performed as described before (2).

Image Processing and Data Analysis. ***Puncta quantification.*** For quantification of puncta, we used the Volocity image analysis software, version 4.4 (Improvision; PerkinElmer). Fluorescent puncta were identified by defining a threshold of intensity as well as size and shape parameters (see Volocity user guide for a more detailed description of the object identification tasks; http://cellularimaging.perkinelmer.com/pdfs/manuals/VolocityUserGuide.pdf). The same parameters were applied to treated and untreated pairs of slices. After an automatic selection of the objects by the program, a manual inspection was performed, where each object was visually inspected to confirm its validity. Selected objects that did not conform to a certain number of properties (appropriate size, rounded shape, and well-delimited boundaries) were discarded. Data are presented as average number of puncta ± SEM from three independent experiments (two slices per experiment for each condition). Analysis to determine statistical differences was performed using the paired *t* test.

Colocalization between FFN102 and GFP labeling. For striatal slices, we determined object colocalization between the FFN102 and GFP channels using Volocity's "Measure Object Colocalization" task that calculates a colocalization coefficient, which indicates the fraction of the signal above threshold in one channel that exists as colocalized with a second channel (3).

Colocalization coefficients ranging from 0 (none of the signal above threshold in that channel exists as colocalized with the other channel) to 1 (all of the signal above threshold in that channel exists as colocalized with the other channel), for each of the selected objects were then obtained. A colocalization coefficient of 0.5 or higher was considered to be indicative of colocalization. Visual inspection of each object was performed to rule out obvious false positives and false negatives. Results are expressed as percentage of FFN102 objects that colocalize with GFP ± SEM and were calculated from at least three independent experiments (two slices per experiment, 200–250 puncta per slice).

For coronal midbrain slices, cells were considered positive for either fluorophore if their mean fluorescence intensity was above 2× SD of the mean background fluorescence intensity, which was determined in an area devoid of fluorescence signal. The number of cells was manually counted in images from three different positions per area from three different animals (a total nine of images per brain structure).

Activity-dependent release by electrical stimulation in the dorsal striatum. Quantification of activity-dependent destaining was determined using two different methods, both of which produced similar results. For electrical destaining experiments, 2.5-μm *z* stacks were composed of six images, with each image acquired at 0.5-μm intervals. One quantification method made use of the Volocity software. As Volocity cannot correct for shifts in the *z* plane, *z* sections corresponding to the same field of view were manually selected for each of the time points. Selected images were imported into Volocity to allow for *x*–*y* registration correction of the whole time course. The first time point was then used to identify fluorescent puncta (objects) as described above. The mean fluorescence intensity value for each identified object was then calculated by the program for all time points: *x*–*y* location, shape, and size of each object mask were identical throughout all images of the time course. Puncta that moved significantly out of the object mask during the time frame analyzed were discarded. Background intensity defined as the fluorescence intensity in areas of the field of view that exclude puncta and cell bodies was also determined. A mean fluorescence intensity value was then obtained for the background of each image over time, allowing background subtraction for each individual puncta.

The alternative method of image analysis used MacBiophotonics ImageJ for the identification of fluorescent puncta. An in-house written macro was used to correct for movement in the *z* dimension throughout the time course. Registration in *x*–*y* was achieved using the PoorMan3DReg plugin (written by Michael Liebling, University of California, Santa Barbara, as a modification of Philippe Thévenaz's, École Polytechnique Fédérale de Lausanne, Switzerland, plug-in StackReg). The Multiple Thresholds plug-in (created by Damon Poburko, Simon Fraser University, Burnaby, BC, Canada) was then used for fluorescent puncta identification in the image corresponding to the first time point. Upon visual inspection, objects that did not conform to defined properties (appropriate size, rounded shape, and well-delimited boundaries) were discarded, as well as puncta that moved significantly out of the object mask during the time frame analyzed. Occasionally, fluorescent puncta with the above-mentioned characteristics that were not automatically selected by the plug-in were manually selected and added to the list of objects for analysis. The mean intensity values for each object were then obtained for all time points with and without subtraction of background intensity. Background subtraction was achieved using ImageJ's "rolling ball" method (Process/Subtract background).

The fluorescence intensity values obtained for each punctum, using either of the two imaging analysis protocols described above, were plotted as a function of time. Background-subtracted intensity plots revealed that individual puncta could be separated into two overall groups according to their response to stimulation. The first group consisted of puncta that did not significantly respond to stimulation, displaying similar rates of fluorescence loss before and after stimulation onset. The second group consisted of puncta that responded to stimulation with an increased rate in the loss of fluorescence intensity, usually following an exponential decay function. A small fraction of "responding" puncta, however, displayed either a transient increase in fluorescence intensity followed by destaining or a variable lag period between the onset of stimulation and clear fluorescence loss. These kinetics could be explained by an incomplete subtraction of the local background contributing to the fluorescence of those particular puncta, because an average background value of the image is subtracted from each individual puncta at each time point. These puncta could also represent terminals that, for unknown reasons, do indeed exhibit transient fluorescence increases or a lag phase before clear destaining occurs or puncta for which fluorescence loss does not reflect "destaining" but rather random *z* shifts from the field of view or exocytosis-independent changes in fluorescence rundown. As we cannot distinguish between these different possibilities, the small number of puncta that displayed either a transient increase in fluorescence or a lag period before "destaining" were discarded from the analysis described below and only puncta exhibiting clear exponential decay properties were further analyzed and included in the average data of Fig. 5*E*.

Background-subtracted intensity plots for each individual destaining puncta were normalized to the time point before the onset of stimulation (T15) and half-time ($t_{1/2}$) values were calculated using GraphPad Prism 4 by fitting the decay of fluorescence from T15 to T45 with a one-phase exponential decay function. Curves with an R^2 value of <0.6 were discarded. All exponential decay curves exhibited a root mean square error (RMSE) between 0.03 and 0.12 (a RMSE value closer to 0 indicates a better fit). The mean destaining $t_{1/2}$ value was obtained from five independent experiments, each of which contained a minimum of three exponentially destaining puncta, amounting to a total of 32 destaining puncta.

AMPH-induced release of FFN102. For coronal midbrain slices, images were changed into 8-bit and aligned in ImageJ using the Stackreg plug-in (4) with the Rigid Body setting. Regions of interests (ROIs) were outlined around fluorescent cells and the mean intensity was measured. An ROI of an area without any evident FFN102 fluorescence was also outlined in the same images and the mean intensity of this ROI was subtracted from the intensity of the individual fluorescent cells to obtain background-corrected fluorescence. Changes in fluorescence were then quantified by subtracting the raw fluorescence intensity from the initial fluorescence ($\Delta F = F1 - F2$) at the indicated time points. The differences in fluorescence loss between cells of control and treated slices were analyzed with *t* test and the significance level was $P < 0.05$. Normalization was performed only for figure preparation and was accomplished by dividing the fluorescence intensity of the individual cells to their initial fluorescence.

AMPH-induced release of FFN102 in striatal slices was determined using Volocity software in the same manner as described above for activity-dependent release by electrical stimulation.

Pharmacological Characterization of FFN102. The interaction of FFN102 with hDAT is weak as demonstrated in heterologously transfected cells [13.6 ± 4.1% (SEM) inhibition at 10 μM, $n = 3$], performed by Psychoactive Drug Screening Program (PDSP) at University of North Carolina (UNC), Chapel Hill. The screening was performed by the National Institute of Mental Health PDSP (UNC Chapel Hill) according to standard conditions (for detailed procedures, see http://pdsp.med.unc.edu/). The primary screen is used to select ligands that show >50% inhibition of binding of a radiolabeled reference compound at 10 μM concentration at the receptors tested. FFN102 was negative at all examined receptors (<50% inhibition by 10 μM FFN102) except for 5HT2c (K_i ~3 μM). The following receptors and transporters were included in the panel: 5HT1a,b,d,e; 5HT2a,b,c; 5HT3,4,5a,6,7; A2B2, A2B4, A3B2, A3B4, A4B2, A4B4; Adrenergic: Alpha1A, 1B, 1D, 2A, 2B, 2C; Beta1,2,3; BZP; CB1,2; D1–5; DAT, NET, SERT; DOR, KOR, MOR; EP4; H1–4; M1–5; mGluR5 (rat brain); NMDA (PCP site); oxytocin R; PBR; sigma 1; V1A,B, V2.

1. Sawamoto K, et al. (2001) Visualization, direct isolation, and transplantation of midbrain dopaminergic neurons. *Proc Natl Acad Sci USA* 98(11):6423–6428.
2. Zhang H, Sulzer D (2003) Glutamate spillover in the striatum depresses dopaminergic transmission by activating group I metabotropic glutamate receptors. *J Neurosci* 23 (33):10585–10592.
3. Manders EMM, Verbeek FJ, Aten JA (1993) Measurement of co-localization of objects in dual-colour confocal images. *J Microsc* 169:375–382.
4. Thévenaz P, Ruttimann UE, Unser M (1998) A pyramid approach to subpixel registration based on intensity. *IEEE Trans Image Process* 7(1):27–41.

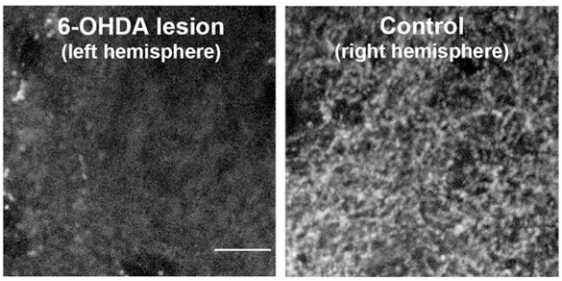

Fig. S1. DAT immunostaining in the dorsal striatum of fixed mouse brain slices visualized with Alexa 488. Low staining for DAT was observed in the injected hemisphere (*Left*) compared with the control hemisphere (*Right*), confirming the loss of dopaminergic terminals after 6-OHDA injection ($n = 2$ animals, 2 slices per condition per animal). (Scale bar, 10 μm.)

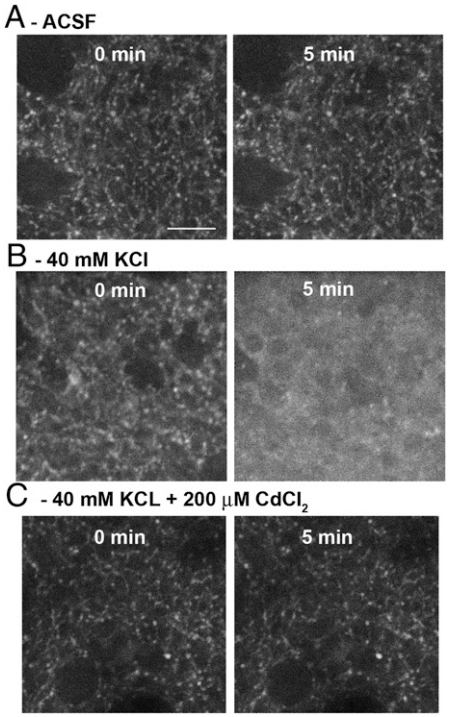

Fig. S2. Visualization of exocytotic release of FFN102 in response to KCl depolarization in the dorsal striatum. (*A*) Representative images of FFN102 in a slice continuously perfused with ACSF at the 0- and 5-min time points. (*B*) FFN102 signal before (*Left*) and 5 min after perfusion with ACSF containing 40 mM KCl (*Right*). (*C*) Fluorescence of FFN102 before (*Left*) and 5 min after perfusion with ACSF containing 40 mM KCl in the presence of 200 μM $CdCl_2$. (Scale bar, 10 μm.)

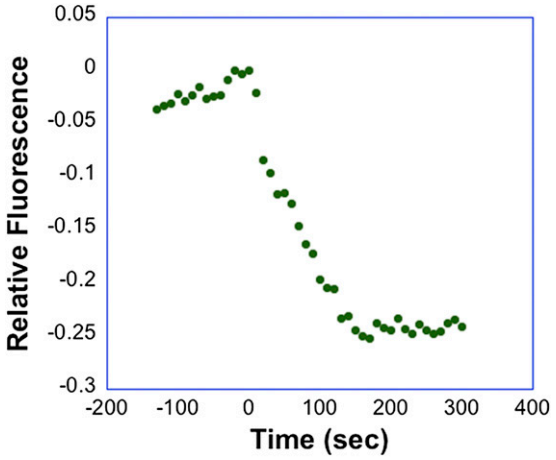

Fig. S3. As an alternative method for analyzing kinetics of destaining puncta (i.e., correcting for background changes), we subtracted the average curve for nondestaining puncta (non–background-subtracted) from the curve for destaining puncta (non–background-subtracted average; selection of destaining and nondestaining puncta performed as described for data shown in Fig. 5*E*). As expected, the resulting curve shows an exponential fluorescence loss similar to that seen in Fig. 5*E* (also lacking the fluorescence increase that immediately follows stimulation in non–background-subtracted traces). Stimulation was initiated at time 0 s.

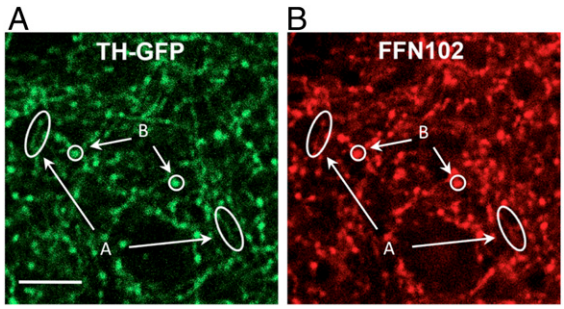

Fig. S4. Similarities in the labeling pattern of GFP and FFN102 in the dorsal striatum of acute mouse brain slices. Fibers (*A*) and puncta (*B*) were observed with both fluorescent markers. (Scale bar, 10 μm.)